Free Radical Biology and Medicine 100 (2016) 43–52

Contents lists available at ScienceDirect

Free Radical Biology and Medicine

journal homepage: www.elsevier.com/locate/freeradbiomed

Real-time and high-throughput analysis of mitochondrial metabolic states in living cells using genetically encoded NAD$^+$/NADH sensors

Yuzheng Zhao [a,b,c,*], Yi Yang [a,b,c,*]

[a] Synthetic Biology and Biotechnology Laboratory, State Key Laboratory of Bioreactor Engineering, Shanghai Collaborative Innovation Center for Biomanufacturing Technology, East China University of Science and Technology, 130 Mei Long Road, Shanghai 200237, China
[b] Optogenetics & Synthetic Biology Interdisciplinary Research Center, CAS Center for Excellence in Brain Science, East China University of Science and Technology, 130 Mei Long Road, Shanghai 200237, China
[c] Shanghai Key Laboratory of New Drug Design, School of Pharmacy, East China University of Science and Technology, 130 Mei Long Road, Shanghai 200237, China

ARTICLE INFO

Article history:
Received 4 February 2016
Received in revised form
21 April 2016
Accepted 30 May 2016
Available online 1 June 2016

Keywords:
Mitochondria
Cytosol
Metabolic state
Genetically encoded fluorescent sensor
Imaging
High-throughput
NADH
NAD$^+$/NADH ratio

ABSTRACT

Mitochondria are central organelles that regulate cellular bioenergetics, biosynthesis, and signaling processes. NADH, a key player in cell metabolism, is often considered as a marker of mitochondrial function. However, traditional methods for NADH measurements are either destructive or unable to distinguish between NADH and NADPH. In contrast to traditional methods, genetically encoded NADH sensors can be used for the real-time tracking and quantitative measurement of subcellular NADH levels in living cells. Therefore, these sensors provide innovative tools and address the limitations of current techniques. We herein summarize the properties of different types of recently developed NADH biosensors, discuss their advantages and disadvantages, and focus on the high-throughput analysis of mitochondrial function by using highly responsive NAD$^+$/NADH sensors.

1. Introduction

Mitochondria are dynamic and heterogeneous organelles, which contain 13 mitochondrial DNA-encoded respiratory chain proteins and more than 1100 nuclear DNA-encoded proteins [1,2]. Mitochondria play central roles in cell metabolism and redox signaling; these organelles are also often referred to as powerhouses of cells and sources of reactive oxygen species (ROS) [3–5]. Mitochondrial disorders are involved in various human diseases, including but not limited to aging, cancer, obesity, diabetes, cardiovascular diseases, and neurodegenerative diseases [2,4,6]. As such, mitochondrial functions in living cells and *in vivo* should be monitored to investigate the pathological processes of such diseases [6,7]. Techniques capable of real-time and high-throughput measuring are highly preferred. This review describes emerging methods to assess cell metabolism in living cells and *in vivo* by using genetically encoded NAD$^+$/NADH sensors.

2. Mitochondrial function and NAD$^+$/NADH

Reduced nicotinamide adenine dinucleotide (NADH) and its oxidized form NAD$^+$ are important coenzymes found in all living cells. More than 700 oxidoreductive enzymes use NAD$^+$ or NADH as cofactors [8]. Redox reactions catalyzed by various NAD(H)-dependent dehydrogenases are vital in energy metabolism, such as glycolysis, tricarboxylic acid (TCA) cycle, and oxidative phosphorylation. In cells, two major NAD$^+$/NADH pools exist: cytosolic and mitochondrial pools. The cytosolic and mitochondrial free NAD$^+$/NADH ratios are 60–600 [9–11] and 4–10 [9,12] in typical eukaryotic cells, respectively. NADH is produced during glucose, fatty acid, and amino acid catabolism (Fig. 1). Glycolysis-derived NADH is transferred to the mitochondria *via* the malate-aspartate and glycerol phosphate shuttle [13] (Fig. 1). NADH molecules are oxidized to generate ATP *via* the mitochondrial respiration chain [14] (Fig. 1).

NADH is a naturally fluorescent molecule in the human body [6,7]. Since the discovery of pyridine nucleotides by Harden and Young [15], the use of NADH as a marker for mitochondrial functions has been described in more than 1000 papers [7]. We and many other researchers showed that both cytosolic or mitochondrial NAD$^+$/NADH redox state responded to metabolic perturbations of almost all major energy metabolism pathways, including glycolysis,

* Corresponding authors at: Synthetic Biology and Biotechnology Laboratory, State Key Laboratory of Bioreactor Engineering, Shanghai Collaborative Innovation Center for Biomanufacturing Technology, East China University of Science and Technology, 130 Mei Long Road, Shanghai 200237, China.
E-mail addresses: yuzhengzhao@ecust.edu.cn (Y. Zhao), yiyang@ecust.edu.cn (Y. Yang).

http://dx.doi.org/10.1016/j.freeradbiomed.2016.05.027
0891-5849/

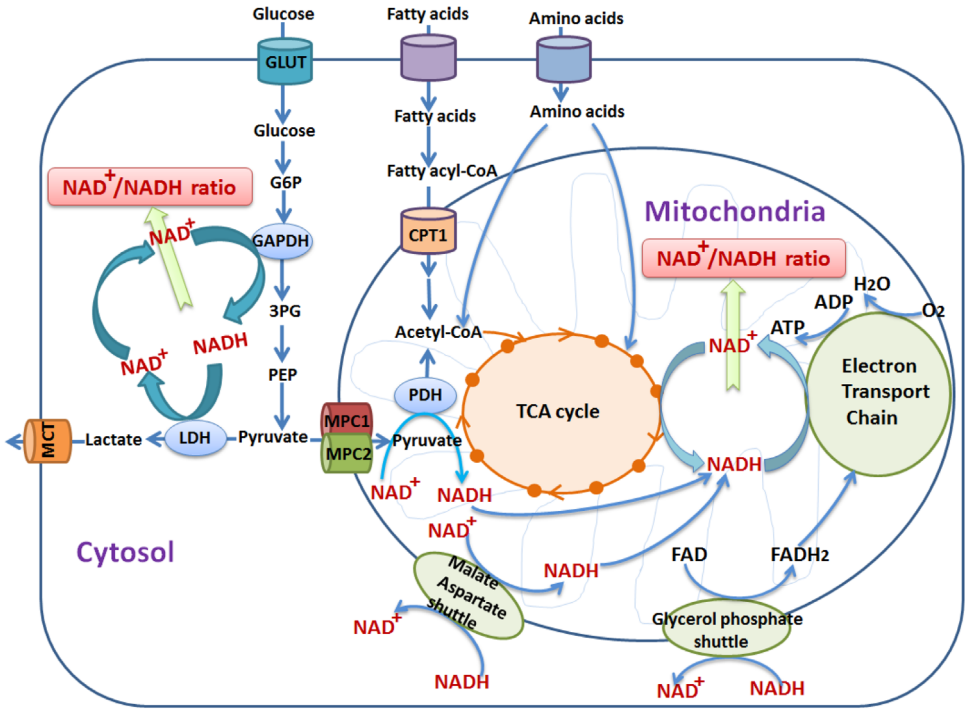

Fig. 1. The central role of NAD^+/NADH in cell metabolism. (NADH from glucose, fatty acid, and amino acid catabolism is oxidized to generate ATP and H_2O by oxidative phosphorylation. NADH produced in glycolysis is transferred to mitochondria *via* the malate-aspartate and glycerol phosphate shuttle. GLUT, glucose transporter type 1; GAPDH, glyceraldehyde-3-phosphate dehydrogenase; LDH, lactate dehydrogenase; MCT, monocarboxylate transporter; MPC1, Mitochondrial Pyruvate Carrier 1; MPC2, Mitochondrial Pyruvate Carrier 2; PDH, pyruvate dehydrogenase; CPT1, carnitine palmitoyl transferase; TCA, tricarboxylic acid cycle.

the malate-aspartate shuttle, TCA cycle, mitochondrial respiration and oxidative stress [13,14,16–23]. Therefore, intracellular NAD^+/NADH redox state can indicate metabolic changes and thus is often considered as a very useful cellular metabolic readout [24–26]. Furthermore, studies also showed that the NAD^+/NADH redox state is closely linked to various physiological or pathological processes, including mitochondrial function, calcium homeostasis, gene expression, cell death, embryonic development, aging, cancer, diabetes, and epilepsy [7,13,24,27–30].

Complementary to NADH fluorescence, mitochondrial functions can also be examined by determining the mitochondrial FAD fluorescence depending on its oxidation-reduction state under various physiological conditions [31–33]. The fluorescence lifetime of protein-bound FAD decreases in the presence of NAD^+ due to intramolecular dynamic quenching in the presence of NAD^+ [31]. This suggests that the lifetime of protein-bound FAD is sensitive to changes in NAD^+ levels [31]. However, FAD fluorescence measurement was not as popular as that of NADH in the metabolic studies due to lower signal and concerns of interference from hemoglobin absorbance [6,7,34]. Therefore, NAD(P)H autofluorescence monitoring is preferred in blood perfused organs [6,7]. Monitoring cytochrome oxidase oxidation-reduction state is another strategy for assessing mitochondrial function. However, cytochrome *c* is not fluorescent and prone to suffering from the interference of blood [6,7].

3. NAD(P)H autofluorescence

The redox dependent optical property of NAD^+/NADH was discovered more than 50 years ago. NADH, as well as its phosphorylated form NADPH, is weakly fluorescent under ultraviolet excitation; by contrast, its oxidized counterpart NAD^+ is not [7,35]. The first detailed study of NADH fluorescence in live cells was conducted in 1957 by Duysens and Amesz, who used yeast cells and algal cells as models [36] (Fig. 2). Britton Chance and Avraham Mayevsky modified and improved intensity- or lifetime-based techniques for NADH fluorescence excited by either single photon (Ex/Em: 350 nm/460 nm) or multiple photons (Ex/Em: 700 nm/460 nm); they also expanded the application of NADH fluorescence to various experimental samples and conditions, including isolated mitochondria, intact cells, tissue slices, and animal organs (Fig. 2) [6,7]. Although monitoring techniques for endogenous NAD(P)H fluorescence have been widely employed, they are limited by several aspects, including low sensitivity, cell injury caused by ultraviolet irradiation, and insufficient resolution between NADH and NADPH. Cytosolic signals are very difficult to separate and measure from intense mitochondrial signals because intrinsic NAD(P)H fluorescence signals mostly originate from the mitochondria. Blacker et al. reported that fluorescence lifetime imaging (FLIM) can be applied to quantitatively differentiate NADPH from NADH (Fig. 2) possibly because bound NADH and bound NADPH exhibit different fluorescence lifetimes inside cells [37]; however, FILM is not technically simple for broad applications. For more details, please also see Duchen's introduction in the same issue of *Free Radical Biology and Medicine* on mitochondrial redox signaling.

Besides NAD(P)H autofluorescence imaging, there are also existing alternative methods to study NAD^+/NADH content in cell lysates, using enzyme cycling assay [38], HPLC [39,40], or HPLC-MS [41]. However, these methods do not allow real-time monitoring of NAD^+/NADH dynamics with a single cell or subcellular resolution, and report the total pools of NAD^+ or NADH originated from a group of cells.

4. Genetically encoded NAD^+/NADH sensors

Compared with endogenous NAD(P)H fluorescence, genetically encoded NAD^+/NADH sensors provide potential alternatives and

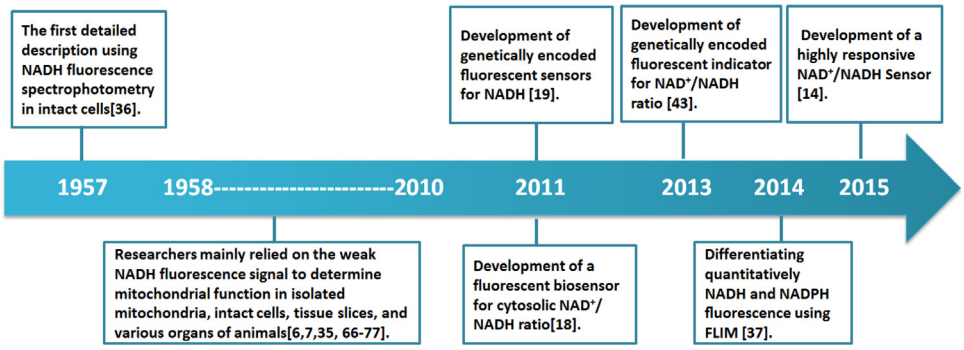

Fig. 2. Historical development of NADH monitoring in living cells and *in vivo*. 1957 – The first detailed description using NADH fluorescence spectrophotometry in intact cells [36]. 1958–2010 – Researchers mainly relied on the weak NADH fluorescence signal to determine mitochondrial function in isolated mitochondria, intact cells, tissue slices, and various organs of animals [6,7,35,66–77]. 2011 – Development of genetically encoded fluorescent sensors for NADH [19]. 2011 – Development of a fluorescent biosensor for cytosolic NAD+/NADH ratio [18]. 2013 – Development of genetically encoded fluorescent indicator for NAD+/NADH ratio [43]. 2014 – Differentiating quantitatively NADH and NADPH fluorescence using FLIM [37]. 2015 – Development of a highly responsive NAD+/NADH sensor [14].

numerous advantages [14,18,19,42]. We and other researchers independently developed genetically encoded NADH sensors, including Frex, Peredox, RexYFP, and SoNar [14,18,19,43], by fusing NADH-binding Rex protein with circularly permuted fluorescent proteins (cpFPs) (Fig. 3 and Table 1). These sensors produce a much higher fluorescence quantum yield than NAD(P)H autofluorescence; therefore, these sensors significantly improve the sensitivity of assays compared with measurements of endogenous NAD(P)H fluorescence. These sensors also specifically detect the NAD^+/NADH redox status without the interference from NADPH, which performs physiological functions distinct from those of NADH. These sensors can be genetically introduced to cells or organisms and conveniently targeted to various subcellular compartments; thus, signals from specific cells and specific subcellular organelles are identified. Among the sensors, Frex and SoNar are sensitive to a dynamic range that exceeds those of other metabolite sensors. They manifest an 800% or 1500% change in fluorescence upon NADH binding or under different NAD^+/NADH ratios [14,19,42] (Table 1); as a result, they can report subtle differences in NADH levels during biological processes. These sensors are ratiometric, that is, they respond to NADH levels differently *via* two excitation wavelengths [14,19]. They can also be made to become ratiometric [18]; consequently, quantitative measurement can be performed because their readouts of the ratio of the two fluorescent channels are irrelevant to sensor expression levels in cells (Table 1). With these sensors, dynamic changes in NAD^+/NADH redox status in the cytosol, nuclei, or mitochondria can be monitored by using various instruments, such as fluorescent microscopes, flow cytometers, or microplate readers. In subsequent sections, the properties and performance of these sensors *in vitro* and *in vivo* are presented. High specificity, brightness, dynamic response, rapid response, and correct measurement range are properties necessary to develop efficient sensors successfully [44–46].

5. Frex

A Frex sensor is designed by fusing Rex from *Bacillus subtilis* (B-Rex) and circularly permuted yellow fluorescent protein (cpYFP) [19] (Fig. 3A). Then, the amino acid residues around the NADH binding pocket are subjected to single site-directed mutagenesis to reduce their affinity to NADH and NAD^+ and to increase their selectivity to NADH over NAD^+. Native B-Rex protein exhibits a high affinity to NADH (K_d=24 nM) [47]. For NADH, Frex yields K_d of approximately 3.7 μM at pH 7.4; this parameter is slightly increased to approximately 11 μM at pH 8.0 (Table 1). For NAD^+, B-Rex produces K_d of approximately 500 μM [19,47]. Frex binding to NAD^+ is negligible [19]. The response of Frex sensor to various NADH concentrations is not significantly affected by the physiological concentrations of free NAD^+ [23]; therefore, Frex measures free NADH levels but not NAD^+/NADH ratio.

Using Frex sensors, we can quantify subcellular NADH concentrations in mammalian cells. The cytosolic free NADH levels of approximately 120 nM are extremely low, as determined by Frex fluorescence. Mitochondrial free NADH level, approximately 30 μM [19], are more than two magnitudes higher, consistent with the view that endogenous NAD(P)H fluorescence signals originate mostly from NADH inside the mitochondria [7]. Under physiological conditions, Frex is largely saturated by NADH in the mitochondrial matrix. A low-affinity mutant of Frex (C3L194K) is then recommended to visualize the increase in mitochondrial NADH levels as induced by mitochondrial respiration inhibitors or hypoxia [19,48]. C3L194K, a Frex mutant with K_d of approximately 50 μM (Table 1), is approximately 35% saturated in the mitochondrial matrix of HEK293 cells. Cytosolic and mitochondrial NADH levels are affected by NADH transport, glucose metabolism, malate-aspartate shuttle activity, electron transport chain function, hypoxia, and redox environment, as monitored by Frex fluorescence [19,48].

Similar to many sensors with a cpYFP moiety, Frex sensors are mainly limited by their pH sensitivity. In the mitochondrial matrix, pH often varies depending on energy metabolism states and ROS generation. cpYFP shares very similar pH dependence with Frex [19]; however, the former is unresponsive to NADH redox state. Therefore, the effects of pH on Frex fluorescence can be corrected by measuring cpYFP fluorescence in parallel experiments [19]. Frex sensors are also limited by their poor folding and weak fluorescence in certain cells, such as primary cells or cells that are uneasily transfected [14]. This may be explained by the fact that the NADH binding domain of Frex was derived from a mesophilic Rex protein, and that the fusion and mutation lowered their stability.

6. Peredox

Peredox sensors were constructed using similar mechanisms to those of Frex sensors except that a pH-insensitive circular permutated T-sapphire fluorescent protein was inserted between the two subunits of the thermophilic Rex from *Thermus aquaticus* (T-Rex) [18] (Fig. 3B). Further mutations were performed to eliminate the pH sensitivity of the sensor. Peredox exhibits a 150% dynamic range, which is much smaller than that of Frex and SoNar sensors (Table 1 and Fig. 4). Peredox was shown to report cytosolic NAD^+/NADH ratio rather than NADH concentration, as NAD^+ competes with NADH for binding. However, the fluorescence

Table 1
Genetically encoded sensors for the detection of intracellular NAD^+/NADH redox state.

Properties	SoNar	Peredox- mCherry	RexYFP	Frex	FrexH	C31194K
Sensor origin	T-Rex	T-Rex	T-Rex	B-Rex	B-Rex	B-Rex
Fluorescent protein	cpYFP	cpT-Sapphire and mCherry	cpYFP	cpYFP	cpYFP	cpYFP
Ex/Em (nm)	420/518; 500/518	400/510; 580/610	490/516	420/518; 500/518	420/518; 500/518	420/518; 500/518
Species sensed	NAD^+/NADH ratio	NAD^+/NADH ratio	NAD^+/NADH ratio	NADH	NADH	NADH
Detection range	0.8–2000 for NAD^+/NADH ratio	80–1320 for NAD^+/NADH ratio	0.045–0.72 μM for NADH	0.15–90 μM for NADH (pH 7.4)	7–230 nM for NADH	5.5–450 μM for NADH
K_d for substrate	$K_{NAD/NADH}$: ~40; K_{NADH}: 0.2 μM	$K_{NAD/NADH}$: ~330	K_{NADH}: ~0.18 μM	K_{NADH}: ~3.7 μM (pH 7.4) or ~11 μM (pH 8.0)	K_{NADH}: ~40 nM	K_{NADH}: ~50 μM (pH 8.0)
Dynamic changes (%)	1500	150	50	800	200	300
Detection mode	Ratiometric	Ratiometric	Intensiometric	Ratiometric	Ratiometric	Ratiometric
pH sensitivity	Resistant[a]	Resistant	Sensitive	Sensitive	Sensitive	Sensitive
Brightness in cells	Strong	Moderate	N.D.	Weak	Weak	Weak
Aggregation in cells	No	Aggregation in cytosol	N.D.	No	No	No
Validated application	Cytosol	Cytosol/Nucleus	Cytosol/Mitochondria	Cytosol/Nucleus/Mitochondria	Cytosol	Mitochondria
References	[14]	[18]	[43]	[19,48]	[19]	[19]

N.D., not determined.
[a] SoNar's fluorescence excited at 420 nm, dynamic range, and $K_{NAD/NADH}$ are pH resistant.

response of Peredox is also dependent on the total pool of NAD^+/NADH because a 3-fold change in the NAD^+ pool size in the physiological range results in a 2-fold change in the sensor midpoint for NAD^+/NADH ratio [18]. This phenomenon is presumptively due to the weak affinity of Peredox to NAD^+. Therefore Peredox cannot strictly indicate an accurate physiologically relevant NAD^+/NADH ratio because the total NAD(H) pool size varies among cell types. For quantitative studies of cellular NAD^+/NADH ratio, the effects of total NAD(H) pool size on the response of Peredox sensor may be calibrated by measuring steady-state fluorescence response of Peredox in the cells depending on the lactate: pyruvate ratio in the extracellular solution, which was then compared to the *in vitro* response of purified Peredox proteins titrated with NAD^+/NADH with a certain pool size (also see Fig. 3C, 3D of Peredox paper) [18]. However, the reliability of such calibration was limited, as it was on the basis of simplified assumptions that extracellular lactate/pyruvate ratio equilibrated with cytosolic lactate/pyruvate ratio, which equilibrated with cytosolic NAD^+/NADH ratio through catalysis of LDH reaction.

The selectivity of Peredox to NADH over NAD^+ is rather high and is roughly 8-fold higher than that of SoNar; therefore, this sensor is suitable for high NAD^+/NADH ratio conditions (Fig. 4). In cancer cells with high glycolytic activity, Peredox appears to be saturated by NADH under normal cell culture conditions with glucose supplementation [14,18] (Fig. 4); as a consequence, the sensor is unable to respond to a further decrease in NAD^+/NADH induced by physiological and pathological conditions, such as hypoxia, mitochondrial dysfunction, and hyperglycemia. Peredox may also be saturated by NADH in the mitochondrial matrix under normal cell culture conditions because of very high NADH levels in the mitochondrial matrix; however, this phenomenon should be further investigated. NADH is also uneasily dissociated from Peredox because of the high affinity; thus, Peredox yields a low off rate and responds more slowly than other sensors do when NADH level decreases [14,18]. In previous study [18], it was also shown that Peredox was already saturated by NADH when cells were incubated with 1 mM glucose, not to mention the normal blood glucose concentration of 5 mM. In our study, the Peredox sensor slightly responded to stimuli when H1299 cells were incubated with high lactate concentrations to mimic the glycolytic state; by contrast, the fluorescence of Peredox decreased to approximately 45% when H1299 cells were incubated with 1 mM pyruvate [14]. The dynamic range of Peredox sensor is 150%; this finding indicates that the maximum decrease in the fluorescence of Peredox is 40% when NAD^+/NADH ratio decreases from infinity to zero. These data also suggest that the Peredox sensor is almost fully saturated by NADH under normal cell culture conditions. This high affinity of Peredox to NADH likely limits its usefulness for *in vivo* applications. In most experiments conducted on Peredox sensors [18], cells are incubated with high lactate and pyruvate levels to increase the cytosolic NAD^+/NADH ratio of the cells until the measurable range of Peredox is reached. The Peredox sensor is intensiometric because it is characterized by one excitation peak and one emission peak. Peredox was fused with mCherry, a red fluorescent protein, to develop sensors with ratiometric readouts. However, this strategy increases the overall size of Peredox and produces aggregates of the sensor in cells [18] (Table 1). Among the genetically encoded sensors for NAD^+/NADH redox states, the Peredox sensor is the most resistant to pH changes in the physiological range. As such, this sensor is suitable for applications under pH-fluctuating conditions. Utilizing Peredox, Yellen et al. measured the cytosolic NAD^+/NADH redox state of several cultured and primary cell types and applied Peredox to high-content image analysis [18].

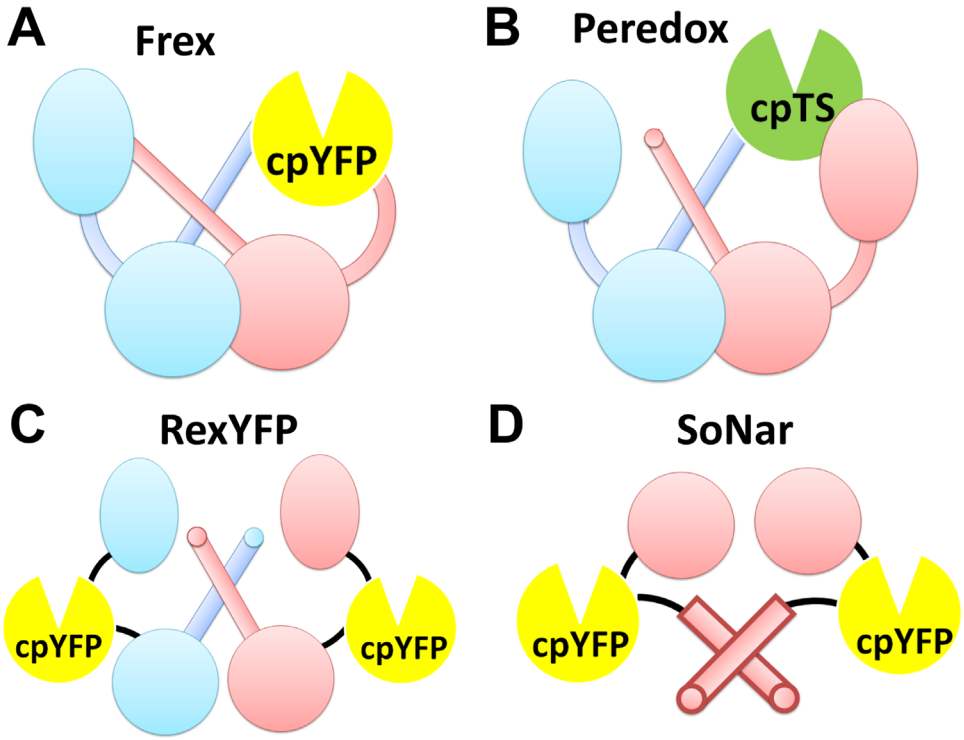

Fig. 3. Design of genetically encoded NADH sensors. (A) Design of Frex, which is a fusion of cpYFP, a complete B-Rex monomer and the NADH-binding of a second B-Rex molecule. Figure from [19]. (B) Design of Peredox, which is a fusion of cpTS and T-Rex dimer. (C) Design of RexYFP, which is a fusion of cpYFP and a complete T-Rex monomer. (D) Design of SoNar, which is a fusion of cpYFP and the NADH-binding domain of T-Rex. Figure from [14].

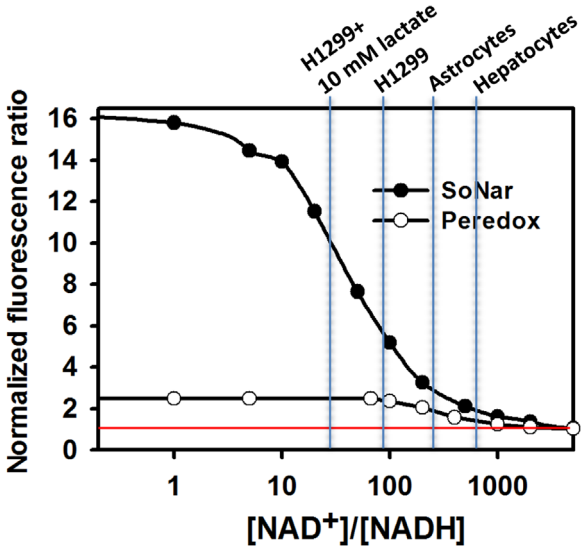

Fig. 4. Responses of SoNar and Peredox to different NAD^+/NADH ratios. Experimental conditions and figure from [14,18].

7. RexYFP

RexYFP sensors were engineered by integrating cpYFP between residues 79 and 80 of the T-Rex monomer *via* short polypeptide linkers (Fig. 3C). These sensors were then used to probe the NAD^+/NADH redox state in the cytoplasm and mitochondrial matrix of cells [43]. The structure of RexYFP is very similar to that of SoNar (Figs. 3C and 3D). However, the former is larger than the latter and is characterized by different cpYFP insertion sites (Figs. 3C and 3D). RexYFP is an intensity-based sensor with a moderate dynamic range (Table 1). Similar to Frex and SoNar, RexYFP is sensitive to pH (Table 1). pH-stimulated factors may be eliminated by normalizing to the signal of a pH sensor with the same chromophore [14,17,19,49]. RexYFP is described in detail in a review written by V. Belousov in the same issue of *Free Radical Biology and Medicine*.

8. SoNar

The above three sensors, Frex, Peredox and RexYFP, do not fulfill all the requirements of an optimal or ideal sensor. Considering the central role NAD^+/NADH play in cell metabolism, just as the calcium signal for neuroscience, it deserves continued development and optimization, to obtain a bright, large dynamic range, and purely NAD^+/NADH ratio-specific sensor for the real-time tracking of the metabolic states of living cells and living animals. Very recently, we developed such a NAD^+/NADH redox sensor, named SoNar, which represents a substantial improvement for NAD^+/NADH ratio measurement in live cells [14]. SoNar was developed by insertion cpYFP to C-terminal loop closing to the ligand binding region of the thermophilic T-Rex, truncating the linker region before or after the cpYFP domain, and removing the DNA-binding domain of T-Rex (Fig. 3D). The SoNar sensor provides significant advantages, are as follows: 1) SoNar is the only genetically encoded sensor that responds to NADH and NAD^+. Previously designed NADH sensors, such as Frex, Peredox, or RexYFP, elicit fluorescence response to the binding of NADH but not to the binding of NAD^+. SoNar exerts a large, opposing fluorescence response to NAD^+ and NADH. Therefore, SoNar can be used as a separate sensor for NADH or NAD^+ for *in vitro* studies when only one of the forms exists. In many important regulatory enzymes and drug targets, such as ADP-ribose polymerases and Sirt family deacylases, NAD^+ functions as a co-substrate, in addition to its role as an electron carrier. SoNar can be used to perform a continuous NAD^+ consumption activity assay of these enzymes. 2) SoNar accurately reports the NAD^+/NADH ratio under

physiological conditions (Fig. 4) and remains unaffected by the total NAD(H) pool. SoNar also exhibits high affinity to NAD^+ (k_d of approximately 5.0 μM) and NADH (k_d of approximately 0.2 μM). Inside cells under physiological conditions, the total intracellular pool of NAD^+ and NADH ranges from 50 μM to 400 μM [20,50–52], which greatly exceeds the dissociation constants of SoNar for NAD^+ and NADH; thus, the sensor could be occupied by either NAD^+ or NADH molecules. Its steady-state fluorescence could also strictly report the NAD^+/NADH ratio rather than the absolute concentrations of either of the two nucleotides. In contrast to SoNar, Frex sensor reports only the NADH level and the Peredox sensor partially presents the NAD^+/NADH ratio. 3) The dynamic range of SoNar is 1500% at different NAD^+/NADH ratios *in vitro* (Fig. 4), and this result is almost 2-fold greater than that of Frex and 10-fold greater than that of Peredox (Table 1). This result is also one order of magnitude higher than that of other metabolite biosensors. Their dynamic ranges are usually from 20% to 150% [42]. With this property, SoNar is among the few most responsive genetically encoded sensors available to date. As such, SoNar can resolve subtle metabolic changes within a broad range of NAD^+/NADH ratio. 4) SoNar sensors exhibit a much more intense fluorescence than Frex does [14] (Table 1). Thus, these sensors perform well in *in vivo* studies involving mammalian models and high-throughput screening. SoNar is also bright and functional in a transgenic zebrafish model (data not shown). This finding supports future applications. Although many sensors have been developed, very few genetically encoded sensors can be used for *in vivo* studies, particularly mammalian models. To our knowledge, none of the previously reported NADH sensors or other metabolite sensors has been reported in mammalian studies.

SoNar sensors, together with mitochondrial-targeted Frex sensors, provide a unique opportunity to assess mitochondrial function *via* different views: cytosolic NADH and mitochondrial NADH. We found that complex I, III, and IV inhibitors increased mitochondrial NADH levels, whereas complex II and malate-aspartate shuttle inhibitor decreased mitochondrial NADH levels (Fig. 5A). Nevertheless, these inhibitors significantly decreased the cytosolic NAD^+/NADH ratio. Therefore, the inhibition of mitochondrial respiration not only affected the mitochondrial NADH redox state but also regulated the cytosolic NADH redox state. In previous study, other NADH sensors also demonstrated that complex I inhibition or the malate-aspartate shuttle inhibition increased cytosolic NADH levels [14,43], in agreement with the results of SoNar. Furthermore, when glucose or lactate was supplemented to the medium, cytosolic NADH rose immediately, whereas it took about 10 min for the raise of mitochondrial NADH level (Figs. 5B and 5C). These results suggested that the NADH concentration in the cytosol is sensitive to environmental changes, while the mitochondria have a strong tendency to maintain physiological NADH homeostasis [19]. Although the free NADH levels in the cytosol is two magnitudes lower than those in the mitochondria [19,49], a comprehensive understanding of mitochondrial and cytosolic NADH level should help identify the pathway perturbed by various inhibitors or energy sources.

Using SoNar, we determined cytosolic NAD^+/NADH ratio in various cells [14], which ranges from 100 to 900 [14,23]. In comparison, intracellular NAD^+/NADH ratio was reported to be 2–10 measured by biochemical methods such as enzyme cycling assay [38], HPLC [39,40], or HPLC-MS [41]. Such differences were due to the fact that those alternative methods cannot distinguish mitochondrial or cytosolic NAD^+/NADH. Cytosolic NADH measurement with these methods easily introduces contaminants from the mitochondrial NADH pool; thus, the cytosolic NADH level is often overestimated.

Two concerns should be emphasized when SoNar is applied to metabolic research. First, SoNar sensors do not permit the direct quantification of NAD^+ or NADH levels separately in living cells or living organisms. Second, its fluorescence excited at 485 nm is sensitive to pH (Fig. 6A), and this characteristic is similar to that observed in other cpYFP-based sensors. Fortunately, its fluorescence excited at 420 nm (Fig. 6D), dynamic range, and $K_{NAD^+/NADH}$ are pH resistant (Figs. 6E and 6F). SoNar displays a 15-fold change in fluorescence with excitation at 485 and 420 nm at different NAD^+/NADH ratios *in vitro*; as such, the sensor is included among the most responsive genetically encoded sensors available to date. By contrast, nearly 2-fold change in fluorescence is detected at an excitation of 485 nm within the physiological pH range of 7.0 to pH 7.4 in the cytosol (Fig. 6A). Thus, pH variations moderately complicate the fluorescence ratio of SoNar. In many circumstances, the effects of pH on SoNar [14] and other cpYFP-based sensors [53–55] are not evident. However, when cytosolic pH fluctuations do occur, SoNar fluorescence can be measured with 420 nm excitation only, at the expense of reduced dynamic range [14] (Fig. 6D). Alternatively, the pH effects on SoNar fluorescence excited at 485 nm may be corrected by measuring SoNar's and cpYFP's fluorescence in parallel because of their very similar pH responses [14] (Fig. 6B). For correction of pH effects with cpYFP, we suggest that the users always measure the fluorescence ratio of cpYFP alone in cells in parallel with measurements in SoNar-expressing cells, and then calculate the pH-corrected ratio(R) of cells as follows: $R = R_{SoNar}/R_{cpYFP}$ (R_{SoNar} and R_{cpYFP}

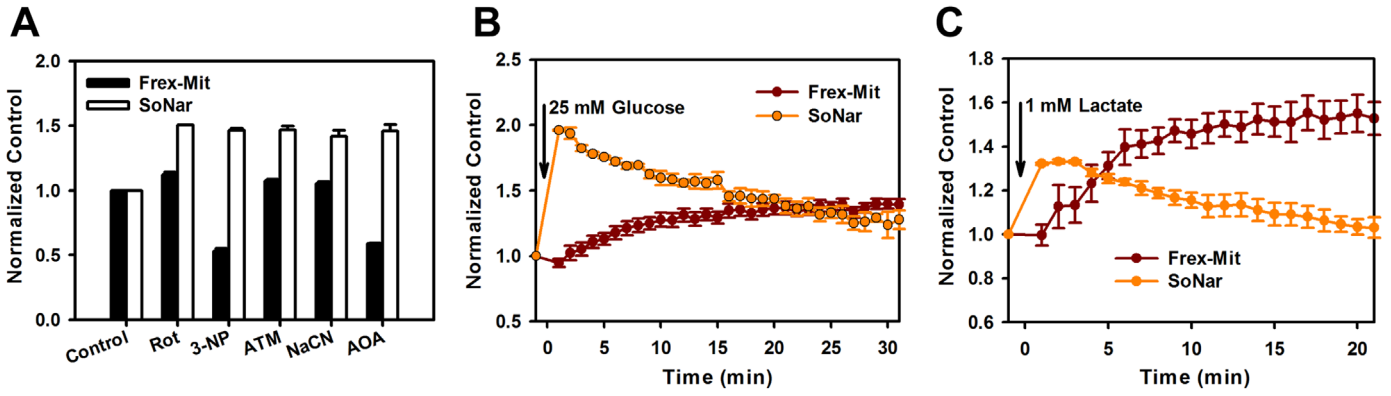

Fig. 5. Responses of Frex-Mit and SoNar to various stimuli in living cells. (A) Fluorescence responses of cells expressing Frex-Mit or SoNar to different mitochondrial inhibitors and the NADH shuttle inhibitor AOA. Cells were treated with inhibitors for 30 min. Frex-Mit fluorescence with excitation at 485 nm was corrected for pH effect by normalization with cpYFP-Mit fluorescence measured in parallel experiments. SoNar fluorescence excited at 420 nm and 485 nm (F420 nm/F485 nm) was normalized to the control condition. Error bars represent SEM. Experimental conditions and figure adapted with permission from [14,19]. (B and C) Fluorescence responses of cells expressing Frex-Mit or SoNar to glucose (B) or lactate (C). Frex-Mit fluorescence with excitation at 485 nm or SoNar fluorescence excited at 420 nm and 485 nm (F420 nm/F485 nm) was normalized to the control condition. Experimental conditions and figure adapted with permission from [14,19].

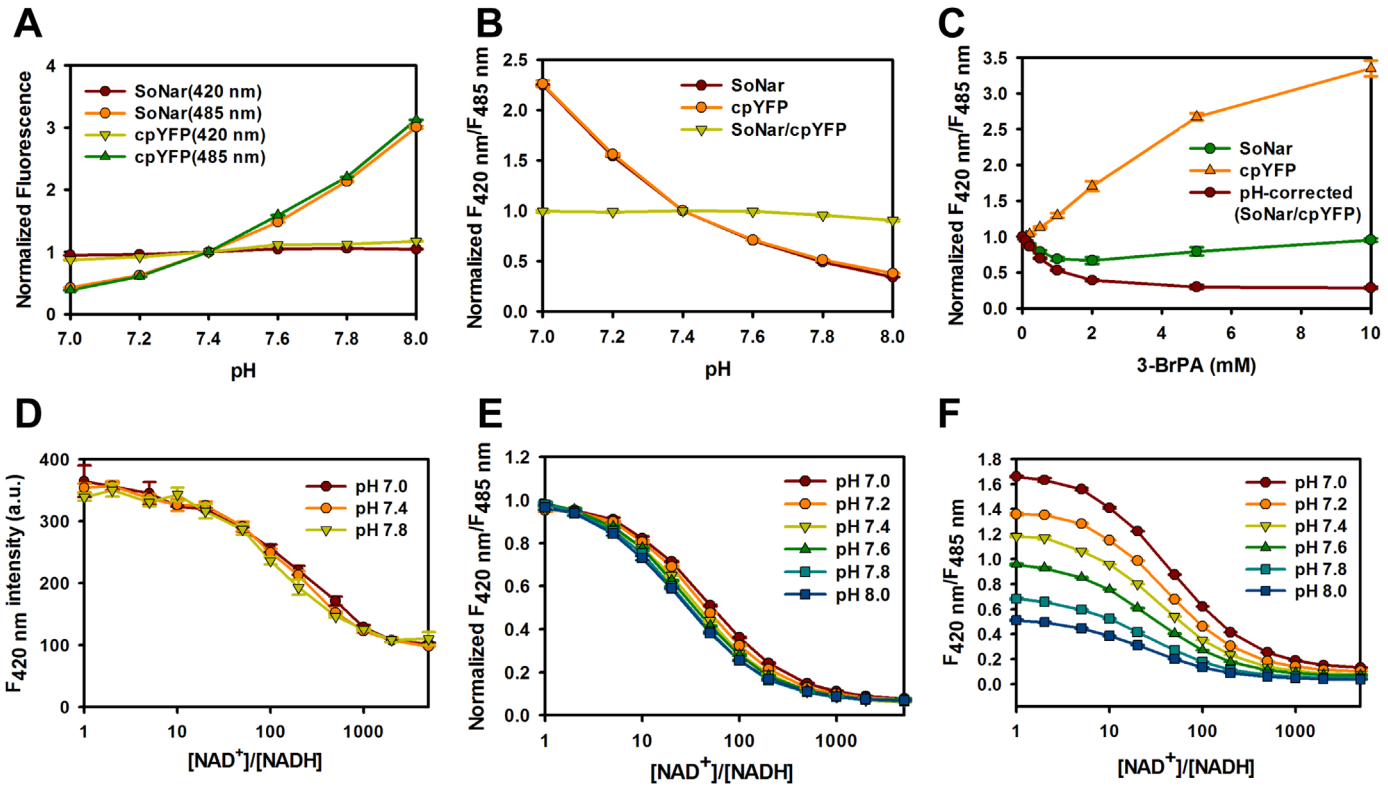

Fig. 6. pH sensitivity and pH effect correction of SoNar. (A) Fluorescence intensities of SoNar and cpYFP with excitation at 420 nm or 485 nm, and emission at 528 nm. Data normalized to the fluorescence at pH 7.4. Figure from [14]. (B) pH-dependency of the excitation ratio 420/485 nm of SoNar and cpYFP. Data normalized to the fluorescence ratio at pH 7.4. Figure from [14]. (C) Dose-dependent response of cytosolic SoNar and cpYFP fluorescence to different concentrations of 3-BrPA in H1299 cells. The dark red line represents the fluorescence response of SoNar corrected for pH effects. Cells were measured immediately after 3-BrPA addition. Data are normalized to samples without 3-BrPA incubation. Figure from [14]. (D) Fluorescence intensity of SoNar when excited at 420 nm plotted against the NAD^+/NADH ratio at the indicated pH. Adapted from [14]. (E and F) Normalized (E) and Un-normalized (F) ratio of SoNar fluorescence excited at 420 nm and 485 nm at the indicated pH plotted against the NAD^+/NADH ratio. For E, the data was normalized to the scale of 0–1 to demonstrate that SoNar dynamic range and $K_{NAD/NADH}$ are pH resistant. For E, Figure from [14]; For F, Adapted from [14].

represent the excitation ratio 420/485 nm for SoNar and cpYFP, respectively). In Fig. 6C, the fluorescence ratio of SoNar was independent of the concentration of 3-BrPA, a glycolysis inhibitor. The artifact was caused by the decrease in pH in the cytosol, as indicated by the cpYFP fluorescence ratio (Fig. 6C). The SoNar fluorescence ratio was normalized by the cpYFP fluorescence ratio to correct this. The pH-corrected SoNar fluorescence ratio is strictly dependent on the concentration of 3-BrPA. Therefore, the inhibition of glycolysis by 3-BrPA markedly increased the cytosolic NAD^+/NADH ratio (Fig. 6C). As a previously used strategy for other pH-sensitive genetically encoded sensors [54,56,57], pH-sensitive dyes or fluorescent proteins can also be used to correct the fluorescence ratio of SoNar.

9. SoNar-based high-throughput analysis of metabolic states

SoNar is a superior tool for high-throughput analysis of metabolic states in living cells and *in vivo* because of its rapid response, high sensitivity, intense fluorescence, and large dynamic range. For SoNar-based high-throughput chemical screening, a general workflow is described in Fig. 7. Briefly, add compounds and cell suspensions into 384-well black flat bottom plate, respectively, and then measure the fluorescence immediately by using a multimode microplate reader with 420 or 485 nm excitation, and 528 nm emission wavelengths. For a more detailed description, please also see our upcoming *Nature Protocols* paper [14]. Typically, for a 384-well plate assay, it generally takes no longer than 1 s to assess the effect of one compound on cell metabolism. However, for a recently reported nuclear magnetic resonance-based screening method, the overall time is approximately 20–35 min per sample [58].

We examined the effect of >5500 compounds on cell metabolism and found that only a small fraction of the screened compounds affected the cytosolic NAD^+/NADH redox states. Among these compounds, protein kinase inhibitor and phosphokinase inhibitor libraries yielded a significant percentage of hits; this finding indicated the regulatory roles of protein phosphorylation in cell metabolism [14]. The most potent compound increasing the NAD^+/NADH ratio, which is also the most potent selective cancer-killing compound, KP372-1, was identified as a potent NQO1-mediated redox cycling agent. KP372-1 induced extreme oxidative stress, two to three orders of magnitude more efficiently than H_2O_2 or thiol oxidants (aldrithiol-2 and diamide). KP372-1 selectively induced cancer cell apoptosis through a mitochondrial pathway, and effectively reduced tumor growth *in vivo*. Another 7 compounds that significantly increased cytosolic NAD^+/NADH ratio and induced cell death, fascaplysin, plumbagin, NSC-95397, PTP CD45 inhibitor, shikonin, LY-83583 and β-lapachone, also produced oxidative stress in the cells. β-lapachone was known to affect cell metabolism by NQO1 and consuming NAD(P)H [59,60], while shikonin was reported to inhibit cancer cell glycolysis by targeting tumor pyruvate kinase M2 [61]. However, to our knowledge, other compounds have never been directly linked to energy metabolism. Of particular note, quite a few compounds among FDA-approved drugs and the NIH clinical collection also affected cellular metabolism. Among them, Troglitazone, Rosiglitazone, and Zaprinast significantly increased the cytosolic NAD^+/NADH ratio. Interestingly, recent studies showed that these compounds were specific inhibitors of the mitochondrial pyruvate carrier (MPC) [62,63]. Therefore, SoNar responded to the MPC

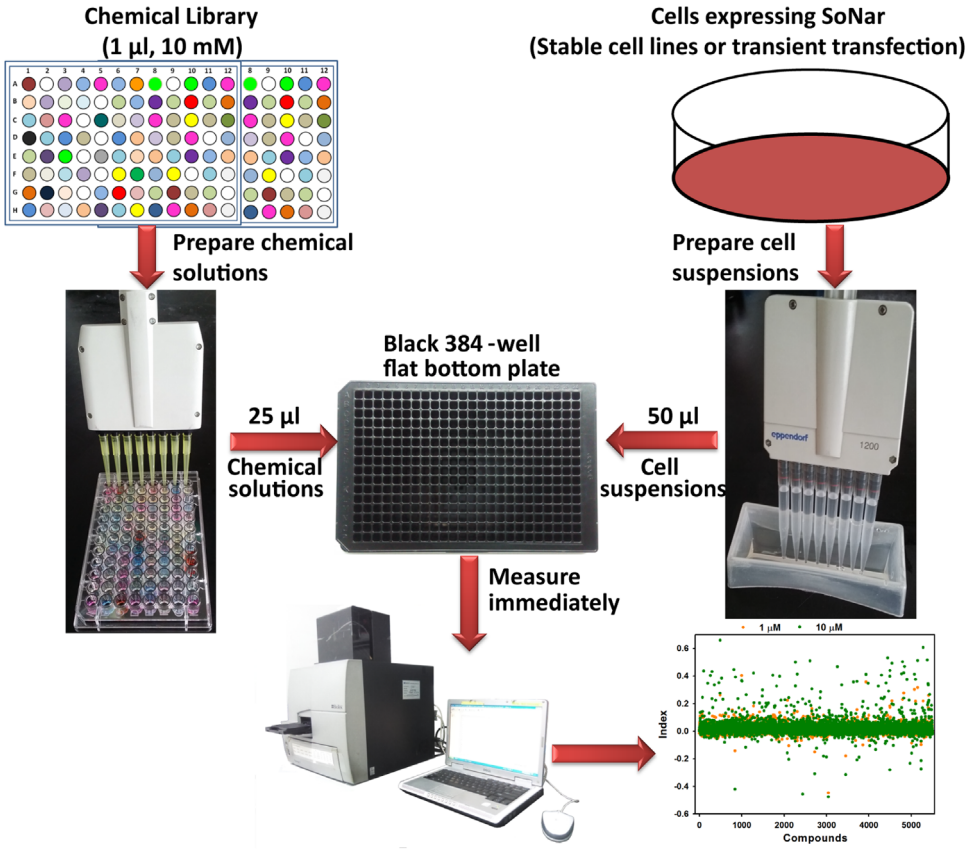

Fig. 7. The workflow of SoNar-based high-throughput chemical screen.

inhibition, which caused the accumulation of pyruvate in the cytosol [64,65] and the increase in the cytosolic NAD^+/NADH ratio. Some hits in our screen may also be due to MPC inhibition. Further studies are underway to identify MPC inhibitors.

10. Concluding remarks

Fluorescent imaging with highly sensitive and specific NAD^+/NADH biosensors can be efficiently used for the real-time profiling of the metabolic states of living cells with single-cell or subcellular resolution. Considering the significant variation of NADH levels in different subcellular compartments, researchers should use sensors with appropriate affinity. We recommended SoNar, FrexH, Peredox, and RexYFP sensors with high affinity for cytosolic or nuclear NADH detection, and Frex and C3L194K sensors with low affinity for mitochondrial NADH detection.

Owing to the physiological and structural complexity of the mitochondria, the NAD^+/NADH sensors together with other redox sensors, such as hyper (H_2O_2 sensors) [53], can help elucidate the mitochondrial redox states. Highly responsive NAD^+ sensors are also preferred. Using such sensors, together with Frex sensors and SoNar sensors, researchers can simultaneously measure three critical parameters, namely, NAD^+, NADH, and their ratio inside cells.

Acknowledgments

This research is supported by the 973 Program (2013CB531200), NSFC (91313301, 31225008, 31071260, 31170815, 31470833, and 91013012), Specialized Research Fund for the Doctoral Program of Higher Education (20100074110010), Shanghai Science and Technology Commission (12JC1402900, 11DZ2260600, 15YF1402600), Dawn Program of the Shanghai Education Commission (11SG31), Lift Engineering for Young Talent of China Association for Science and Technology, State Key Laboratory of Bioreactor Engineering, the 111 Project (B07023), and the Fundamental Research Funds for the Central Universities.

References

[1] S.B. Vafai, V.K. Mootha, Mitochondrial disorders as windows into an ancient organelle, Nature 491 (2012) 374–383.
[2] J. Nunnari, A. Suomalainen, Mitochondria: in sickness and in health, Cell 148 (2012) 1145–1159.
[3] S.E. Weinberg, N.S. Chandel, Targeting mitochondria metabolism for cancer therapy, Nat. Chem. Biol. 11 (2015) 9–15.
[4] D.C. Chan, Mitochondria: dynamic organelles in disease, aging, and development, Cell 125 (2006) 1241–1252.
[5] S.S. Sabharwal, P.T. Schumacker, R.O.S. Mitochondrial, in cancer: initiators, amplifiers or an Achilles' heel? Nat. Rev. Cancer 14 (2014) 709–721.
[6] A. Mayevsky, E. Barbiro-Michaely, Use of NADH fluorescence to determine mitochondrial function in vivo, Int. J. Biochem. Cell Biol. 41 (2009) 1977–1988.
[7] A. Mayevsky, G.G. Rogatsky, Mitochondrial function in vivo evaluated by NADH fluorescence: from animal models to human studies, Am. J. Physiol. Cell Physiol. 292 (2007) C615–C640.
[8] F. Sun, C. Dai, J. Xie, X. Hu, Biochemical issues in estimation of cytosolic free NAD/NADH ratio, PLoS One 7 (2012) e34525.
[9] D.H. Williamson, P. Lund, H.A. Krebs, The redox state of free nicotinamide-adenine dinucleotide in the cytoplasm and mitochondria of rat liver, Biochem. J. 103 (1967) 514–527.
[10] Q. Zhang, D.W. Piston, R.H. Goodman, Regulation of corepressor function by nuclear NADH, Science 295 (2002) 1895–1897.
[11] L.R. Stein, S. Imai, The dynamic regulation of NAD metabolism in mitochondria, Trends Endocrinol. Metab. 23 (2012) 420–428.
[12] R.L. Veech, L.V. Eggleston, H.A. Krebs, The redox state of free nicotinamide-adenine dinucleotide phosphate in the cytoplasm of rat liver, Biochem. J. 115 (1969) 609–619.
[13] K. Eto, Y. Tsubamoto, Y. Terauchi, T. Sugiyama, T. Kishimoto, N. Takahashi,

N. Yamauchi, N. Kubota, S. Murayama, T. Aizawa, Y. Akanuma, S. Aizawa, H. Kasai, Y. Yazaki, T. Kadowaki, Role of NADH shuttle system in glucose-induced activation of mitochondrial metabolism and insulin secretion, Science 283 (1999) 981–985.
[14] Y. Zhao, Q. Hu, F. Cheng, N. Su, A. Wang, Y. Zou, H. Hu, X. Chen, H.M. Zhou, X. Huang, K. Yang, Q. Zhu, X. Wang, J. Yi, L. Zhu, X. Qian, L. Chen, Y. Tang, J. Loscalzo, Y. Yang, SoNar, a highly responsive NAD(+)/NADH sensor, allows high-throughput metabolic screening of anti-tumor agents, Cell Metab. 21 (2015) 777–789.
[15] H. A, Y. W, Alcoholic ferment of yeast-juice. Part II. Co-ferment of yeast-juice), Proc. R. Soc. Lond. B Biol. Sci. B78 (1906) 369–375.
[16] Y. Zhao, Y. Yang, Profiling metabolic states with genetically encoded fluorescent biosensors for NADH, Curr. Opin. Biotechnol. 31 (2015) 86–92.
[17] D.S. Bilan, M.E. Matlashov, A.Y. Gorokhovatsky, C. Schultz, G. Enikolopov, V.V. Belousov, Genetically encoded fluorescent indicator for imaging NAD (+)/NADH ratio changes in different cellular compartments, Biochim. Biophys. Acta 1840 (2014) 951–957.
[18] Y.P. Hung, J.G. Albeck, M. Tantama, G. Yellen, Imaging cytosolic NADH-NAD(+) redox state with a genetically encoded fluorescent biosensor, Cell Metab. 14 (2011) 545–554.
[19] Y. Zhao, J. Jin, Q. Hu, H.M. Zhou, J. Yi, Z. Yu, L. Xu, X. Wang, Y. Yang, J. Loscalzo, Genetically encoded fluorescent sensors for intracellular NADH detection, Cell Metab. 14 (2011) 555–566.
[20] G.H. Patterson, S.M. Knobel, P. Arkhammar, O. Thastrup, D.W. Piston, Separation of the glucose-stimulated cytoplasmic and mitochondrial NAD(P)H responses in pancreatic islet beta cells, Proc. Natl. Acad. Sci. USA 97 (2000) 5203–5207.
[21] Q. Gao, M.S. Wolin, Effects of hypoxia on relationships between cytosolic and mitochondrial NAD(P)H redox and superoxide generation in coronary arterial smooth muscle, Am. J. Physiol. Heart Circ. Physiol. 295 (2008) H978–H989.
[22] K.A. Kasischke, H.D. Vishwasrao, P.J. Fisher, W.R. Zipfel, W.W. Webb, Neural activity triggers neuronal oxidative metabolism followed by astrocytic glycolysis, Science 305 (2004) 99–103.
[23] Y. Zhao, A. Wang, Y. Zou, N. Su, J. Loscalzo, Y. Yang, In vivo monitoring of cellular energy metabolism using SoNar, a highly responsive sensor for NAD +/NADH redox state, Nat. Protoc. 11 (2016) 1345–1359.
[24] S.J. Lin, L. Guarente, Nicotinamide adenine dinucleotide, a metabolic regulator of transcription, longevity and disease, Curr. Opin. Cell Biol. 15 (2003) 241–246.
[25] R.H. Houtkooper, C. Canto, R.J. Wanders, J. Auwerx, The secret life of NAD+: an old metabolite controlling new metabolic signaling pathways, Endocr. Rev. 31 (2010) 194–223.
[26] C. Canto, K.J. Menzies, J. Auwerx, NAD(+) metabolism and the control of energy homeostasis: a balancing act between mitochondria and the nucleus, Cell Metab. 22 (2015) 31–53.
[27] W. Ying, NAD^+/NADH and $NADP^+$/NADPH in cellular functions and cell death: regulation and biological consequences, Antioxid. Redox Signal. 10 (2008) 179–206.
[28] R. Dumollard, Z. Ward, J. Carroll, M.R. Duchen, Regulation of redox metabolism in the mouse oocyte and embryo, Development 134 (2007) 455–465.
[29] M. Garriga-Canut, B. Schoenike, R. Qazi, K. Bergendahl, T.J. Daley, R.M. Pfender, J.F. Morrison, J. Ockuly, C. Stafstrom, T. Sutula, A. Roopra, 2-Deoxy-D-glucose reduces epilepsy progression by NRSF-CtBP-dependent metabolic regulation of chromatin structure, Nat. Neurosci. 9 (2006) 1382–1387.
[30] Q. Zhang, S.Y. Wang, A.C. Nottke, J.V. Rocheleau, D.W. Piston, R.H. Goodman, Redox sensor CtBP mediates hypoxia-induced tumor cell migration, Proc. Natl. Acad. Sci. USA 103 (2006) 9029–9033.
[31] M.C. Skala, K.M. Riching, A. Gendron-Fitzpatrick, J. Eickhoff, K.W. Eliceiri, J. G. White, N. Ramanujam, In vivo multiphoton microscopy of NADH and FAD redox states, fluorescence lifetimes, and cellular morphology in precancerous epithelia, Proc. Natl. Acad. Sci. USA 104 (2007) 19494–19499.
[32] S. Huang, A.A. Heikal, W.W. Webb, Two-photon fluorescence spectroscopy and microscopy of NAD(P)H and flavoprotein, Biophys. J. 82 (2002) 2811–2825.
[33] F. Bartolome, A.Y. Abramov, Measurement of mitochondrial NADH and FAD autofluorescence in live cells, Methods Mol. Biol. 1264 (2015) 263–270.
[34] V.V. Ghukasyan, A.A. Heikal, Natural biomarkers for cellular metabolism: biology, techniques, and applications, 2014.
[35] B. Chance, P. Cohen, F. Jobsis, B. Schoener, Intracellular oxidation-reduction states in vivo, Science 137 (1962) 499–508.
[36] L.N. Duysens, J. Amesz, Fluorescence spectrophotometry of reduced phosphopyridine nucleotide in intact cells in the near-ultraviolet and visible region, Biochim. Biophys. Acta 24 (1957) 19–26.
[37] T.S. Blacker, Z.F. Mann, J.E. Gale, M. Ziegler, A.J. Bain, G. Szabadkai, M. R. Duchen, Separating NADH and NADPH fluorescence in live cells and tissues using FLIM, Nat. Commun. 5 (2014) 3936.
[38] C. Canto, Z. Gerhart-Hines, J.N. Feige, M. Lagouge, L. Noriega, J.C. Milne, P. J. Elliott, P. Puigserver, J. Auwerx, AMPK regulates energy expenditure by modulating NAD+ metabolism and SIRT1 activity, Nature 458 (2009) 1056–1060.
[39] L.K. Klaidman, A.C. Leung, J.D. Adams Jr., High-performance liquid chromatography analysis of oxidized and reduced pyridine dinucleotides in specific brain regions, Anal. Biochem. 228 (1995) 312–317.
[40] D.P. Jones, Determination of pyridine dinucleotides in cell extracts by high-performance liquid chromatography, J. Chromatogr. 225 (1981) 446–449.
[41] R. Cerutti, E. Pirinen, C. Lamperti, S. Marchet, A.A. Sauve, W. Li, V. Leoni, E. A. Schon, F. Dantzer, J. Auwerx, C. Viscomi, M. Zeviani, NAD(+)-dependent activation of Sirt1 corrects the phenotype in a mouse model of mitochondrial disease, Cell Metab. 19 (2014) 1042–1049.
[42] Y. Zhao, Y. Yang, Profiling metabolic states with genetically encoded fluorescent biosensors for NADH, Curr. Opin. Biotechnol. 31C (2015) 86–92.
[43] D.S. Bilan, M.E. Matlashov, A.Y. Gorokhovatsky, C. Schultz, G. Enikolopov, V. V. Belousov, Genetically encoded fluorescent indicator for imaging NAD/NADH ratio changes in different cellular compartments, Biochim. Biophys. Acta 1840 (2013) 951–957.
[44] A.E. Palmer, Y. Qin, J.G. Park, J.E. McCombs, Design and application of genetically encoded biosensors, Trends Biotechnol. 29 (2011) 144–152.
[45] A. Ibraheem, R.E. Campbell, Designs and applications of fluorescent protein-based biosensors, Curr. Opin. Chem. Biol. 14 (2010) 30–36.
[46] J. Zhang, R.E. Campbell, A.Y. Ting, R.Y. Tsien, Creating new fluorescent probes for cell biology, Nat. Rev. Mol. Cell Biol. 3 (2002) 906–918.
[47] E. Wang, M.C. Bauer, A. Rogstam, S. Linse, D.T. Logan, C. von Wachenfeldt, Structure and functional properties of the Bacillus subtilis transcriptional repressor Rex, Mol. Microbiol. 69 (2008) 466–478.
[48] Y. Zhao, Y. Yang, Frex and FrexH: Indicators of metabolic states in living cells, Bioeng. Bugs 3 (2012) 181–188.
[49] Y. Zhao, Y. Yang, J. Loscalzo, Real-time assessment of the metabolic profile of living cells with genetically encoded NADH sensors, Methods Enzymol. 542 (2014) 349–367.
[50] K. Yamada, N. Hara, T. Shibata, H. Osago, M. Tsuchiya, The simultaneous measurement of nicotinamide adenine dinucleotide and related compounds by liquid chromatography/electrospray ionization tandem mass spectrometry, Anal. Biochem. 352 (2006) 282–285.
[51] H. Yang, T. Yang, J.A. Baur, E. Perez, T. Matsui, J.J. Carmona, D.W. Lamming, N. C. Souza-Pinto, V.A. Bohr, A. Rosenzweig, R. de Cabo, A.A. Sauve, D.A. Sinclair, Nutrient-sensitive mitochondrial NAD+ levels dictate cell survival, Cell 130 (2007) 1095–1107.
[52] Q. Yu, A.A. Heikal, Two-photon autofluorescence dynamics imaging reveals sensitivity of intracellular NADH concentration and conformation to cell physiology at the single-cell level, J. Photochem. Photobiol. B 95 (2009) 46–57.
[53] V.V. Belousov, A.F. Fradkov, K.A. Lukyanov, D.B. Staroverov, K.S. Shakhbazov, A.V. Terskikh, S. Lukyanov, Genetically encoded fluorescent indicator for intracellular hydrogen peroxide, Nat. Methods 3 (2006) 281–286.
[54] J. Berg, Y.P. Hung, G. Yellen, A genetically encoded fluorescent reporter of ATP: ADP ratio, Nat. Methods 6 (2009) 161–166.
[55] T. Nagai, A. Sawano, E.S. Park, A. Miyawaki, Circularly permuted green fluorescent proteins engineered to sense Ca2, Proc. Natl. Acad. Sci. USA 98 (2001) 3197–3202.
[56] Y. Li, R.W. Tsien, pHTomato, a red, genetically encoded indicator that enables multiplex interrogation of synaptic activity, Nat. Neurosci. 15 (2012) 1047–1053.
[57] M. Tantama, Y.P. Hung, G. Yellen, Imaging intracellular pH in live cells with a genetically encoded red fluorescent protein sensor, J. Am. Chem. Soc. 133 (2011) 10034–10037.
[58] S. Tiziani, Y. Kang, J.S. Choi, W. Roberts, G. Paternostro, Metabolomic high-content nuclear magnetic resonance-based drug screening of a kinase inhibitor library, Nat. Commun. 2 (2011) 545.
[59] E.A. Bey, M.S. Bentle, K.E. Reinicke, Y. Dong, C.R. Yang, L. Girard, J.D. Minna, W. G. Bornmann, J. Gao, D.A. Boothman, An NQO1- and PARP-1-mediated cell death pathway induced in non-small-cell lung cancer cells by beta-lapachone, Proc. Natl. Acad. Sci. USA 104 (2007) 11832–11837.
[60] J.J. Pink, S.M. Planchon, C. Tagliarino, M.E. Varnes, D. Siegel, D.A. Boothman, NAD(P)H: quinone oxidoreductase activity is the principal determinant of beta-lapachone cytotoxicity, J. Biol. Chem. 275 (2000) 5416–5424.
[61] J. Chen, J. Xie, Z. Jiang, B. Wang, Y. Wang, X. Hu, Shikonin and its analogs inhibit cancer cell glycolysis by targeting tumor pyruvate kinase-M2, Oncogene 30 (2011) 4297–4306.
[62] A.S. Divakaruni, S.E. Wiley, G.W. Rogers, A.Y. Andreyev, S. Petrosyan, M. Loviscach, E.A. Wall, N. Yadava, A.P. Heuck, D.A. Ferrick, R.R. Henry, W. G. McDonald, J.R. Colca, M.I. Simon, T.P. Ciaraldi, A.N. Murphy, Thiazolidinediones are acute, specific inhibitors of the mitochondrial pyruvate carrier, Proc. Natl. Acad. Sci. USA 110 (2013) 5422–5427.
[63] J. Du, W.M. Cleghorn, L. Contreras, K. Lindsay, A.M. Rountree, A.O. Chertov, S. J. Turner, A. Sahaboglu, J. Linton, M. Sadilek, J. Satrustegui, I.R. Sweet, F. Paquet-Durand, J.B. Hurley, Inhibition of mitochondrial pyruvate transport by zaprinast causes massive accumulation of aspartate at the expense of glutamate in the retina, J. Biol. Chem. 288 (2013) 36129–36140.
[64] N.M. Vacanti, A.S. Divakaruni, C.R. Green, S.J. Parker, R.R. Henry, T.P. Ciaraldi, A. N. Murphy, C.M. Metallo, Regulation of substrate utilization by the mitochondrial pyruvate carrier, Mol. Cell 56 (2014) 425–435.
[65] R. Lerchundi, I. Fernandez-Moncada, Y. Contreras-Baeza, T. Sotelo-Hitschfeld, P. Machler, M.T. Wyss, J. Stobart, F. Baeza-Lehnert, K. Alegria, B. Weber, L. F. Barros, NH4(+) triggers the release of astrocytic lactate via mitochondrial pyruvate shunting, Proc. Natl. Acad. Sci. USA 112 (2015) 11090–11095.
[66] B. Chance, C.M. Connelly, A method for the estimation of the increase in concentration of adenosine diphosphate in muscle sarcosomes following a contraction, Nature 179 (1957) 1235–1237.
[67] B. Chance, H. Baltscheffsky, Respiratory enzymes in oxidative phosphorylation. VII. Binding of intramitochondrial reduced pyridine nucleotide, J. Biol. Chem. 233 (1958) 736–739.
[68] C. B, J. F, Changes in fluorescence in a frog sartorius muscle following a twitch, Nature 184 (1959) 195–196.
[69] B. Chance, D. Jamieson, H. Coles, Energy-linked pyridine nucleotide reduction:

inhibitory effects of hyperbaric oxygen in vitro and in vivo, Nature 206 (1965) 257–263.
[70] A. Mayevsky, B. Chance, A new long-term method for the measurement of NADH fluorescence in intact rat brain with chronically implanted cannula, Adv. Exp. Med. Biol. 37A (1973) 239–244.
[71] A. Mayevsky, B. Chance, Intracellular oxidation-reduction state measured in situ by a multichannel fiber-optic surface fluorometer, Science 217 (1982) 537–540.
[72] A. Mayevsky, A. Doron, T. Manor, S. Meilin, N. Zarchin, G.E. Ouaknine, Cortical spreading depression recorded from the human brain using a multiparametric monitoring system, Brain Res. 740 (1996) 268–274.
[73] M. Simonovich, E. Barbiro-Michaely, A. Mayevsky, Real-time monitoring of mitochondrial NADH and microcirculatory blood flow in the spinal cord, Spine (Phila Pa 1976) 33 (2008) 2495–2502.
[74] A. Mayevsky, S. Meilin, T. Manor, N. Zarchin, J. Sonn, Optical monitoring of NADH redox state and blood flow as indicators of brain energy balance, Adv. Exp. Med. Biol. 471 (1999) 133–140.
[75] A. Mayevsky, Brain NADH redox state monitored in vivo by fiber optic surface fluorometry, Brain Res. 319 (1984) 49–68.
[76] A. Mayevsky, B. Chance, Multisite measurements of NADH redox state from cerebral cortex of the awake animal, Adv. Exp. Med. Biol. 159 (1983) 143–155.
[77] A. Mayevsky, D.L. Sclarksy, Correlation of brain NADH redox state, K+, PO2 and electrical activity during hypoxia, ischemia and spreading depression, Adv. Exp. Med. Biol. 159 (1983) 129–141.